Imbalanced Activation of Wnt-/β-Catenin-Signaling in Liver Endothelium Alters Normal Sinusoidal Differentiation

Philipp-Sebastian Koch [1,2*†], Kajetan Sandorski [1,2†], Joschka Heil [1,2], Christian D. Schmid [1,2], Sina W. Kürschner [1,2], Johannes Hoffmann [1,2], Manuel Winkler [1,2], Theresa Staniczek [1,2], Carolina de la Torre [3], Carsten Sticht [3], Kai Schledzewski [1,2], Makoto Mark Taketo [4], Felix A. Trogisch [2,5], Joerg Heineke [2,5], Cyrill Géraud [1,2,6], Sergij Goerdt [1,2] and Victor Olsavszky [1,2]

[1] Department of Dermatology, Venereology and Allergology, University Medical Center and Medical Faculty Mannheim, Heidelberg University and Center of Excellence in Dermatology, Mannheim, Germany, [2] European Center for Angioscience, Medical Faculty Mannheim, Heidelberg University, Mannheim, Germany, [3] Next Generation Sequencing Core Facility, Medical Faculty Mannheim, Heidelberg University, Mannheim, Germany, [4] Division of Experimental Therapeutics, Graduate School of Medicine, Kyoto University, Kyoto, Japan, [5] Department of Cardiovascular Physiology, Medical Faculty Mannheim, Heidelberg University, Mannheim, Germany, [6] Section of Clinical and Molecular Dermatology, Department of Dermatology, Venereology and Allergology, University Medical Center and Medical Faculty Mannheim, Heidelberg University, Mannheim, Germany

Endothelial wingless-related integration site (Wnt)-/β-catenin signaling is a key regulator of the tightly sealed blood–brain barrier. In the hepatic vascular niche angiokine-mediated Wnt signaling was recently identified as an important regulator of hepatocyte function, including the determination of final adult liver size, liver regeneration, and metabolic liver zonation. Within the hepatic vasculature, the liver sinusoidal endothelial cells (LSECs) are morphologically unique and functionally specialized microvascular endothelial cells (ECs). Pathological changes of LSECs are involved in chronic liver diseases, hepatocarcinogenesis, and liver metastasis. To comprehensively analyze the effects of endothelial Wnt-/β-catenin signaling in the liver, we used endothelial subtype-specific *Clec4g-iCre* mice to generate hepatic ECs with overexpression of Ctnnb1. In the resultant *Clec4g-iCre*$^{tg/wt}$;*Ctnnb1(Ex3)*$^{fl/wt}$ (*Ctnnb1*$^{OE-EC}$) mice, activation of endothelial Wnt-/β-catenin signaling resulted in sinusoidal transdifferentiation with disturbed endothelial zonation, that is, loss of midzonal LSEC marker lymphatic vessel endothelial hyaluronic acid receptor 1 (Lyve1) and enrichment of continuous EC genes, such as cluster of differentiation *(CD)34* and *Apln*. Notably, gene set enrichment analysis revealed overrepresentation of brain endothelial transcripts. Activation of endothelial Wnt-/β-catenin signaling did not induce liver fibrosis or alter metabolic liver zonation, but *Ctnnb1*$^{OE-EC}$ mice exhibited significantly increased plasma triglyceride concentrations, while liver lipid content was slightly reduced. Ctnnb1 overexpression in arterial ECs of the heart has been reported previously to cause cardiomyopathy. As *Clec4g-iCre* is active in a subset of cardiac ECs, it was not unexpected that *Ctnnb1*$^{OE-EC}$ mice showed reduced

overall survival and cardiac dysfunction. Altogether, balanced endothelial Wnt-/β-catenin signaling in the liver is required for normal LSEC differentiation and for maintenance of normal plasma triglyceride levels.

Keywords: mice, liver, liver sinusoidal endothelial cells, endothelial cells, triglycerides

INTRODUCTION

Liver sinusoidal endothelial cells (LSECs) lining the hepatic sinusoids are a prime example for organ-specific endothelial differentiation. They belong to the group of discontinuous ECs characterized by an incomplete basement membrane and the presence of large fenestrations without diaphragm. LSECs exhibit unique molecular, phenotypic, and functional features and are known to instruct the hepatic vascular niche by cellular interactions and the secretion of paracrine-acting factors called angiokines (Nolan et al., 2013; Augustin and Koh, 2017). For example, LSECs were identified to control liver regeneration by angiocrine wingless-related integration site 2 (Wnt2) and hepatocyte growth factor (Hgf) signaling (Ding et al., 2010; Cao et al., 2017; Zhang et al., 2020). Other highly specialized functions include immunological processes, such as tolerance and defense mechanisms and the clearance of noxious factors from the circulation by a repertoire of scavenger receptors (Schledzewski et al., 2011; Wittlich et al., 2017; Shetty et al., 2018). Interestingly, pathological changes of these highly specialized ECs were shown to contribute to severe liver diseases ranging from steatohepatitis to liver cirrhosis and from hepatocarcinogenesis to liver metastasis (Kostallari and Shah, 2016). During disease processes, LSECs are known to transdifferentiate toward a capillary phenotype revealing a loss of fenestrations and formation of a basement membrane, which is termed "sinusoidal capillarization," thereby aggravating disease progression (Schaffner and Popper, 1963; Lalor et al., 2006). However, the molecular and signaling mechanisms driving sinusoidal capillarization still await detailed analysis.

Notably, recent work by our group could identify the transcription factor GATA-binding factor 4 (GATA4) as a molecular master regulator for LSEC differentiation during liver development and in liver homeostasis. LSEC-restricted deletion of *Gata4* was shown to cause transformation of discontinuous liver sinusoids into continuous capillaries. This sinusoidal transformation in the fetal liver inhibited homing of hematopoietic stem and progenitor cells into the fetal liver resulting in fatal anemia (Geraud et al., 2017), while *Gata4* deletion in the mature vasculature caused hepatopathy and perisinusoidal liver fibrosis (Winkler et al., 2021). A special form of liver sinusoidal capillarization was also demonstrated when endothelial Notch signaling was enhanced resulting in a partial loss of LSEC-specific markers and increased the expression of continuous endothelial cell (CEC) markers; however, lacking the formation of a solid basement membrane or liver fibrogenesis (Wohlfeil et al., 2019).

Another highly conserved transduction pathway known to be involved in several important biological processes, such as liver development, vascular and hepatic differentiation, and tissue homeostasis is the Wnt-/β-catenin signaling pathway (Decaens et al., 2008; Daneman et al., 2009; Wild et al., 2020). In the liver vasculature, Wnt2 was identified as an LSEC-associated molecule with autocrine growth effects (Klein et al., 2008; Geraud et al., 2010), and also as an angiocrine regulator of liver regeneration (Ding et al., 2010). In the meantime, angiocrine Wnt signaling in the liver has become even more important. Hepatic endothelial cells (ECs) not only express Wnt2, they also express Wnt9b, Wnt ligand secretion mediator (Wls), and Wnt potentiator R-Spondin 3 (Geraud et al., 2010; Rocha et al., 2015). These factors are indispensable for the formation of a Wnt-dependent pericentral hepatocyte subpopulation. Loss of this Wnt-signaling machinery results in decreased liver size, perturbations of liver zonation, metabolic maturation, and impaired liver regeneration capacity (Rocha et al., 2015; Wang et al., 2015; Planas-Paz et al., 2016; Leibing et al., 2018; Preziosi et al., 2018).

Considering EC morphogenesis and specification, Wnt signaling emerged as a major contributor in the past decades (Choi et al., 2012). ECs not only express intracellular Wnt molecules and their corresponding Frizzled receptors, but also β-catenin-dependent transcription factors (Masckauchan et al., 2005; Deb, 2014). Hereby, it was shown that β-catenin induces arterialization and loss of venous fate of the embryonic vasculature during development (Duarte et al., 2004; Corada et al., 2010). Moreover, in vascular beds of the central nervous system Wnt-signaling is a key regulator of the integrity of the highly sealed blood–brain barrier (BBB) by controlling the formation of tight junction (TJ) molecules and solute transporters (Liebner et al., 2008; Zhou et al., 2014; Tran et al., 2016; Profaci et al., 2020). LSECs, on the other hand, do not typically express TJs, since permeability and cell trafficking are facilitated by open fenestrations (Geraud et al., 2012). Constitutive activation of β-catenin in the highly permeable ECs of the circumventricular organs in the brain resulted in the expression of BBB markers and downregulation of non-BBB vasculature markers (Benz et al., 2019; Wang et al., 2019). As our study and other previous studies have shown that Wnt2 is a LSEC-specific growth and differentiation factor required for liver regeneration and that autocrine Wnt/β-catenin signaling cross-stimulates the angiogenetic vascular endothelial growth factor receptor 2 pathway, we hypothesized that unbalanced canonical endothelial Wnt signaling in the liver might also impair LSEC differentiation and LSEC-mediated liver function. To test this hypothesis, we generated a novel mouse line with constitutive β-catenin overactivation in LSECs by crossing *Ctnnb1-Ex3*$^{fl/wt}$ with EC subtype-specific *Clec4g-iCre*$^{tg/wt}$ mice (Wohlfeil et al., 2019).

MATERIALS AND METHODS

Animals

To generate endothelial subtype-specific Ctnnb1 gain-of-function (GOF) mice ($Ctnnb1^{OE-EC}$), $Clec4g\text{-}iCre^{tg/wt}$ ($Tg(Clec4g\text{-}icre)1.1Sgoe$) (Wohlfeil et al., 2019) were crossed with $Ctnnb1(Ex3)^{fl/wt}$ ($Ctnnb1^{tm1Mmt}$) (Harada et al., 1999) mice. Specificity of Cre-activity was analyzed in crosses of $Clec4g\text{-}iCre^{tg/wt}$ transgenic mice with $R26YFP$ ($B6.129X1$-$Gt(ROSA)26Sortm1(EYFP)Cos/J$) [JAX 006148] (Srinivas et al., 2001) reporter animals. All animals were housed under specific pathogen-free conditions in an animal facility (Heidelberg University). Animal experiments were performed in accordance with Federal Animal Regulations and were institutionally approved by the district government Karlsruhe and performed under institutional guidelines. Mice were sacrificed by cervical dislocation. Liver, heart, kidney, lung, spleen, brain, and intestine weights were measured, and tissue samples were either embedded in the optimum cutting temperature compound (Sakura, Alphen aan den Rijn, The Netherlands) and frozen in liquid nitrogen or fixed in 4% paraformaldehyde at 4°C.

Isolation of Primary Murine LSECs

Livers, pooled from two mice, were perfused in situ via the portal vein with a 0.05% collagenase containing amino acid/saccharide calcium-deprived medium (C2674, Sigma–Aldrich, Taufkirchen, Germany), dissected, mechanically minced, digested at 38°C in a collagenase/Gey's balanced salt solution (G9779, Sigma–Aldrich) and filtered through a 250 μm mesh. Cells were separated by a 35% Nycodenz (1002424, Axis-Shield, Alere Technologies, Oslo, Norway) gradient. Next, LSECs were isolated by magnetic-activated cell sorting using anti-CD146 MicroBeads (ME-9F1, 130-092-007, Miltenyi Biotech, Bergisch Gladbach, Germany) according to the instructions of the manufacturers.

Quantitative Reverse-Transcription PCR

RNA was extracted from primary ECs using EZNA Total-RNA-Kit I (OMEGA Biotec, Norcross, GA, United States). Complementary DNA (cDNA) was synthesized with RevertAid H-Minus M-MuLV Reverse Transcriptase (ThermoScientific, Waltham, MA, United States). Quantitative PCR was performed on a qTOWER 3 G touch thermal cycler (Analytik Jena) using innuMIX qPCR SyGreen Sensitive (845-AS-1310200, Analytik Jena, Jena, Germany). Normalized expression values were calculated using the Pfaffl method considering amplification efficiency values determined by standard curves (Pfaffl, 2001).

RNA in situ Hybridization

Liver tissue was sectioned at 4 μm. RNA in situ hybridization (ISH) was conducted using RNAscope 2.5 HD Red (322350, Advanced Cell Diagnostics, Newark, CA, United States) kits with mouse-specific probes against the positive control mouse $Ppib$ ($Cyclophilin\ B$) gene, $Mus\ musculus$ (Mm)-$Bmp2$-E3-Channel 1 (1545–2347 NM_007553.3), Mm-Hgf-Channel 1 (1120–2030 NM_010427.4), Mm-$Wnt2$-Channel 1 (857–2086 NM_023653.5), Mm-$Wnt9b$-Channel 1 (706–1637 NM_011719.4), Mm-$Stab1$-Channel 1 (488-1320 NM_138672.2),

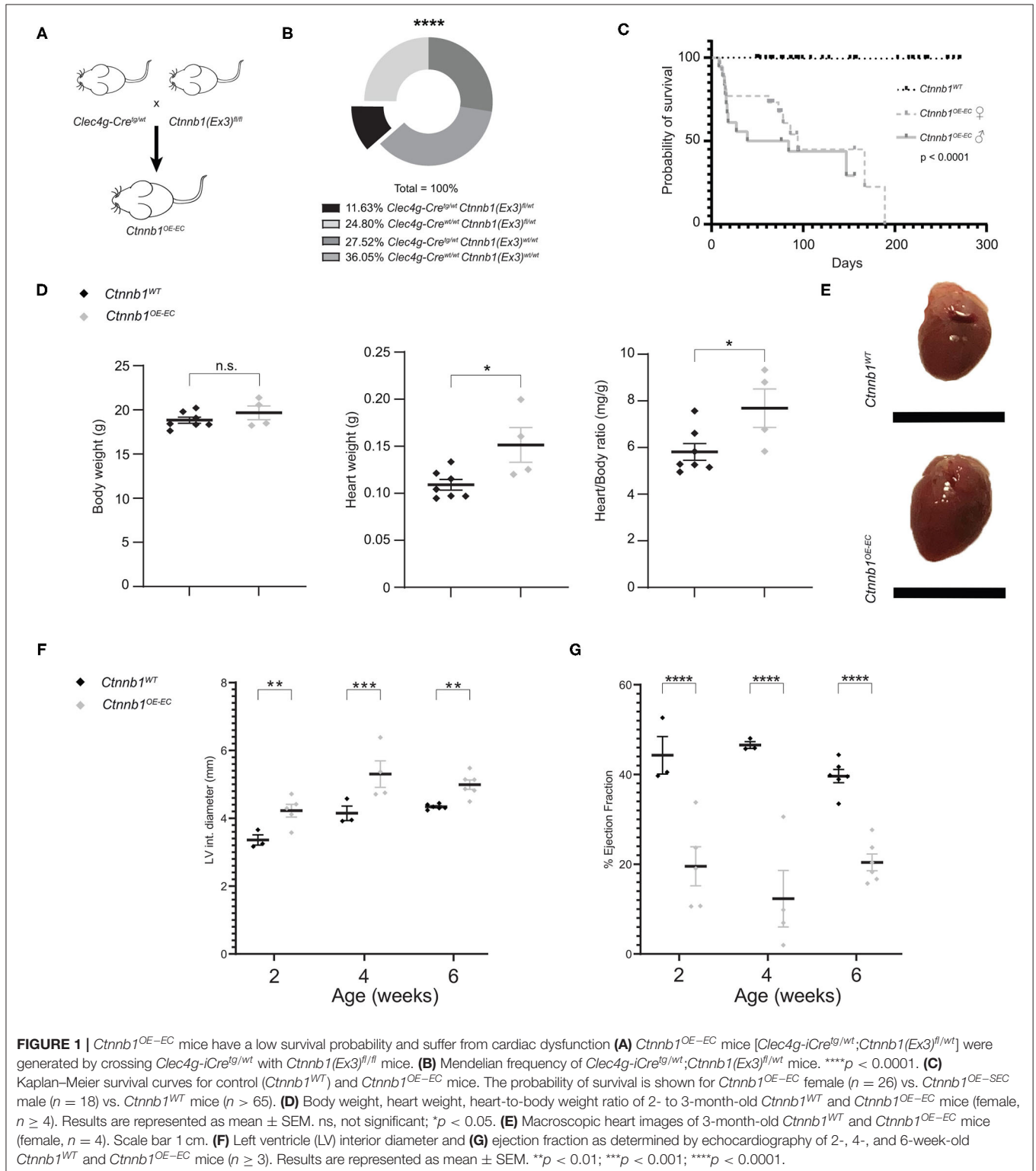and Mm-$Stab2$-Channel 1 (4249–5075 NM_138673.2) according to the protocols of the manufacturer.

Histology and Immunofluorescence

Tissue samples fixed by 4% paraformaldehyde at room temperature for 48–72 h, were subsequently transferred into phosphate-buffered saline (PBS), dehydrated in a graded alcohol series, and embedded in paraffin. Paraffin-embedded tissues were sectioned in 4 μm. For hematoxylin & eosin (H&E), periodic acid–Schiff (PAS), Oil Red O (ORO), Prussian blue, and Sirius red staining, samples were processed according to the standard protocols provided by the manufacturer. For immunofluorescence (IF), cryosections (7 μm) were air-dried, fixed in 4% paraformaldehyde (PFA) or acetone, rehydrated in PBS (A0964.9050, VWR International, Radnor, PA, United States) and blocked in 5% donkey serum (017-000-121, Dianova, Hamburg, Germany) in PBS for 30 min. Primary antibodies were incubated overnight at 4°C. Sections were washed three times in PBS before incubation with appropriate Alexa Fluor–coupled secondary antibodies for 45 min at room temperature. Paraffin-embedded sections were baked at 60°C overnight, after which they were deparaffinized with xylol and rehydrated using ethanol in decreasing concentrations. Antigen retrieval of tissue sections was carried out with epitope retrieval solution (Zytomed Systems, Berlin, Germany) at either pH 6, 8, or 9. Primary antibody was incubated for 2 h at room temperature or overnight at 4°C. Sections were washed three times in PBS before incubation of appropriate secondary antibodies for 1 h at room temperature. Nuclei were counterstained with 4′,6-diamidin-2-phenylindol (DAPI) (D1306, Thermo Fisher Scientific, Waltham, MA, United States). Finally, sections were thoroughly washed in PBS before mounting with Dako fluorescent mounting medium (Dako, Agilent technologies, Santa Clara, CA, United States). Sections were photographed with ECLIPSE Ci microscope (Nikon, Alzenau, Bavaria, Germany) or ECLIPSE Ni-E microscope (Nikon). Immunofluorescence images were acquired in a sequential mode as a series of z-axis images and processed with NIS-Elements AR 5.02 (Nikon Instruments, Tokyo, Japan) and ImageJ 1.52e software (NIH, Bethesda, MD, United States). Using NIS-Elements AR 5.02, images were background corrected (rolling ball 7.5 pixels), deconvoluted, and focused to one plane.

For the quantification of IF images, three representative areas per sample were chosen. For each image, binary masks of the representative channels were created using automated threshold functions (Otsu, MaxEntropy) in ImageJ. The resulting binary masks were quantified for the area, or the number of particles (10-infinite pixels) using ImageJ functions "Measure" and "Analyze Particles." The "Mean gray value" represents the sum of the gray values of all the pixels within the selected images divided by the number of all pixels. For Ki-67 quantification, only Ki-67 staining was included that overlaid with DAPI-positive nucleus staining to exclude unspecific signal. To this end, we used the "Image Calculator" in ImageJ with "AND" as operator for Ki-67 and DAPI channels. For quantification of RNA ISH or ORO images, three representative areas per sample were chosen. RGB images were split into separate

channels corresponding to three determined colors by using the "Color deconvolution" command in ImageJ. The images displaying the region of interest were further processed by setting

color thresholds. Finally, the area of particles (>30 pixels) was measured, analyzed, and calculated in percentage (%) of the whole image area.
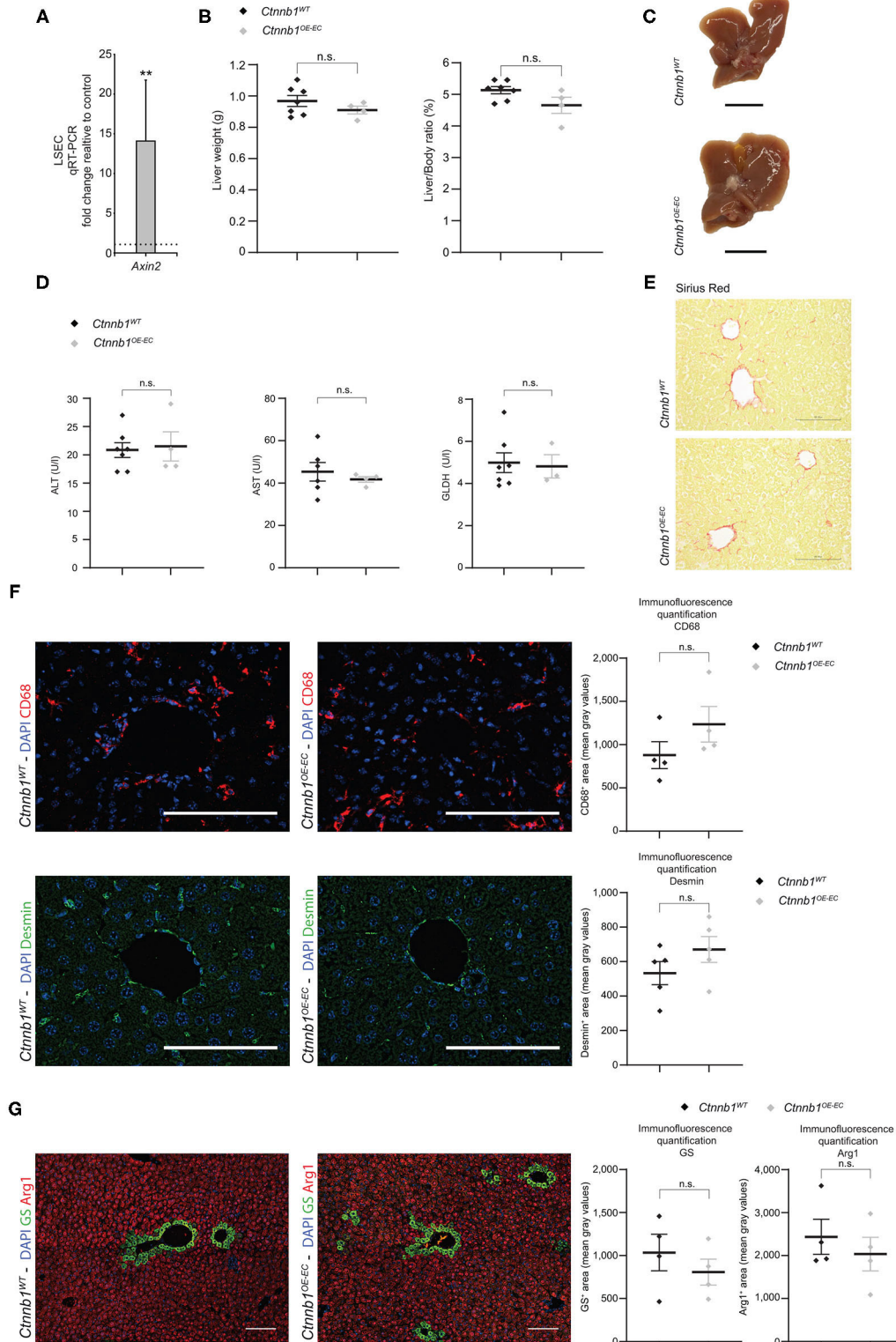

FIGURE 1 | $Ctnnb1^{OE-EC}$ mice have a low survival probability and suffer from cardiac dysfunction **(A)** $Ctnnb1^{OE-EC}$ mice [$Clec4g-iCre^{tg/wt}$;$Ctnnb1(Ex3)^{fl/wt}$] were generated by crossing $Clec4g-iCre^{tg/wt}$ with $Ctnnb1(Ex3)^{fl/fl}$ mice. **(B)** Mendelian frequency of $Clec4g-iCre^{tg/wt}$;$Ctnnb1(Ex3)^{fl/wt}$ mice. ****$p < 0.0001$. **(C)** Kaplan–Meier survival curves for control ($Ctnnb1^{WT}$) and $Ctnnb1^{OE-EC}$ mice. The probability of survival is shown for $Ctnnb1^{OE-EC}$ female ($n = 26$) vs. $Ctnnb1^{OE-SEC}$ male ($n = 18$) vs. $Ctnnb1^{WT}$ mice ($n > 65$). **(D)** Body weight, heart weight, heart-to-body weight ratio of 2- to 3-month-old $Ctnnb1^{WT}$ and $Ctnnb1^{OE-EC}$ mice (female, $n \geq 4$). Results are represented as mean ± SEM. ns, not significant; *$p < 0.05$. **(E)** Macroscopic heart images of 3-month-old $Ctnnb1^{WT}$ and $Ctnnb1^{OE-EC}$ mice (female, $n = 4$). Scale bar 1 cm. **(F)** Left ventricle (LV) interior diameter and **(G)** ejection fraction as determined by echocardiography of 2-, 4-, and 6-week-old $Ctnnb1^{WT}$ and $Ctnnb1^{OE-EC}$ mice ($n \geq 3$). Results are represented as mean ± SEM. **$p < 0.01$; ***$p < 0.001$; ****$p < 0.0001$.

FIGURE 2 | Hepatic endothelial *Ctnnb1* overactivation does not lead to hepatopathy and fibrosis. **(A)** qRT-PCR for axis inhibition protein 2 (*Axin2*) of cDNA from freshly isolated LSECs of 2-months-old *Ctnnb1^{OE−EC}* mice compared to corresponding *Ctnnb1^{WT}* controls ($n = 3$). β-Actin was used as housekeeping gene. **p < 0.01. **(B)** Liver weight, liver-to-body weight ratio of 2- to 3-month-old *Ctnnb1^{WT}* and *Ctnnb1^{OE−EC}* mice (female, $n \geq 4$). Results are represented as mean ± SEM. ns,

(Continued)

FIGURE 2 | not significant. **(C)** Macroscopic liver images of 3-month-old *Ctnnb1*^{WT} and *Ctnnb1*$^{OE-EC}$ mice (female, $n = 4$). Scale bar 1 cm. **(D)** Liver enzymes [aspartate aminotransferase (AST), alanine aminotransferase (ALT), and glutamate dehydrogenase (GLDH)] in serum of 2- to 3-month-old female *Ctnnb1*^{WT} and *Ctnnb1*$^{OE-EC}$ mice ($n \geq 3$). Results are represented as mean ± SEM. n.s., not significant. **(E)** Sirius red staining of liver sections of 2- to 3-month-old male *Ctnnb1*^{WT} and *Ctnnb1*$^{OE-EC}$ mice ($n = 4$). Scale bar 100 μm. **(F)** Immunofluorescence (IF) staining of DAPI, CD68 and Desmin, and CD68 and Desmin quantification in the liver of 2- to 3-month-old female *Ctnnb1*^{WT} and *Ctnnb1*$^{OE-EC}$ mice ($n \geq 4$). Scale bar 100 μm. Results are represented as mean ± SEM. ns, not significant. **(G)** IF staining of DAPI, glutamine synthetase (GS) and arginase (Arg1), and GS and Arg1 quantification in the liver of 2- to 3-month-old *Ctnnb1*^{WT} and *Ctnnb1*$^{OE-EC}$ mice ($n = 4$). Scale bar 100 μm. Results are represented as mean ± SEM. ns, not significant.

Antibodies

Primary antibodies: rat anti-Endomucin (14-5851-82, eBioscience, San Diego, CA, United States), goat anti-Lyve1 (AF2125, R&D Systems, Minneapolis, MN, United States), rat anti-mouse/human GATA-4 (14-9980-82, Thermo Fisher Scientific), rat anti-mouse CD68 (137002, BioLegend, San Diego, CA, United States), rabbit anti-Desmin (ab15200, Abcam, Cambridge, Cambs., UK), rabbit anti-glutamine synthetase (G2781, Sigma–Aldrich, Taufkirchen, Bavaria, Germany), goat anti-arginase I (sc-18351, Santa Cruz Biotechnology, Dallas, TX, United States), rat anti-Ki67 (14-5698-82, eBioscience), polyclonal rabbit anti- green fluorescent protein/yellow fluorescent protein (YFP) (A11122, Molecular Probes, Eugene, OR, United States), rat anti-CD31 (102502, BioLegend), SMA-antibody (ab5694, Abcam), goat anti-CD32b (AF1460, R&D Systems), rabbit anti-Collagen type I (R1038, Acris, Hiddenhausen, North Rhine-Westphalia, Germany), rabbit anti-Collagen type III alpha 1 chain (R1040, Acris), rabbit anti-Collagen IV (GTX19808, Genetex, Irvine, CA, United States), rabbit anti-Cyp2E1 (HPA009128, Sigma–Aldrich), rabbit anti-Claudin 5 (34-1600, Thermo Fisher Scientific), goat anti-Podocalyxin (AF1556, R&D Systems), rabbit anti-Cav1 (N-20, Santa Cruz Biotechnology), rabbit anti- intracellular adhesion molecule 1 (ICAM1) (10020-1-AP, Proteintech, Rosemont, IL, United States), goat anti-mouse vascular endothelial (VE)-cadherin (AF1002, R&D Systems), goat anti- vascular cell adhesion molecule (VCAM)-1/CD106 (AF643, R&D Systems). Secondary antibodies: Alexa-Fluor 488, Alexa-Fluor 647, and cyanine 3-conjugated secondary antibodies were purchased from Dianova (Hamburg, Germany).

Microarray Processing and Statistical Analysis

Gene expression profiling was performed using arrays MoGene-2_0-st from Affymetrix (Santa Clara, CA, United States). Biotinylated antisense cDNA and arrays hybridization were performed according to the recommendations of the manufacturer using the GeneChip WT Plus Reagent Kit and the GeneChip Hybridization, Wash and Stain Kit (both from Thermo Fisher Scientific). A Custom CDF Version 22 with ENTREZ-based gene definitions was used to annotate the arrays. The raw fluorescence intensity was robust multiarray analysis background corrected and values were normalized applying quantile normalization. Differential gene expression was analyzed with the one-way-ANOVA, using a commercial software package SAS JMP15 Genomics, version10, from SAS (SAS Institute, Cary, NC, United States). A false-positive rate of $a = 0.05$ with FDR correction was taken as the level of significance.

To determine whether defined lists (or sets) of genes exhibit a statistically significant bias in their distribution, we performed a gene set enrichment analysis (GSEA). GSEA (Subramanian et al., 2005) was carried out using R 3.6.1. clusterProfiler 3.12.0 (Yu et al., 2012), fgsea 1.10.0 (Korotkevich et al., 2021), the molecular signatures database (MSigDB) v6.2 hallmark gene set collection (Liberzon et al., 2015), and self-defined gene lists were used. Gene lists for LSECs and CECs were used as previously described (Winkler et al., 2021). The gene set for brain ECs was defined using published single-cell RNA seq data (Sabbagh et al., 2018). Inclusion criteria were fold change ≥ 2 for brain *vs.* liver ECs and at least 10 transcripts per million in liver ECs to exclude less-expressed genes. Overrepresentation analysis (ORA) of Gene Ontology terms was performed with the enrichR (Chen et al., 2013) package in R 3.6.1 for all significantly regulated genes. Heatmaps were created with the ComplexHeatmap package (Gu et al., 2016).

The raw and normalized gene expression profiling data have been deposited in the NCBI Gene Expression Omnibus and are accessible through GEO Series accession number GSE175777 (https://www.ncbi.nlm.nih.gov/geo/query/acc.cgi?acc=GSE175777).

Blood Parameters

Serum was analyzed for the following routine parameters: alanine aminotransferase (ALA), aspartate aminotransferase (AST), and glutamate dehydrogenase (GLDH), cholesterol, triglycerides, glucose, and total protein (Roche cobas c 311 analyser, Roche Diagnostics, Basel, Switzerland).

Hepatic Triglycerides

Snap frozen liver tissue (100 mg) was homogenized in 5% NP-40 solution (74385, Merck) and heated for 5 min in a shaking dry incubator (ThermoMixer C, Eppendorf, Hamburg, Germany) at 80–100°C. After cooling to room temperature, the heating was repeated in order to solubilize all triglycerides. After centrifugation for 2 min at top speed (Centrifuge 5417 R, Eppendorf) the supernatant was diluted 10-fold in distilled water and used to determine the triglyceride content based on the protocol of the Triglyceride Quantification Colorimetric/Fluorometric Kit manufacturer (K622, BioVision, Mountain View, CA, United States).

Transthoracic Echocardiography

For echocardiography, mice were anesthetized with 0.5–1.0% isoflurane and placed on a heating pad to maintain body temperature. Non-invasive, echocardiographic parameters were recorded with a linear 50 MHz transducer (Vevo 3100 system
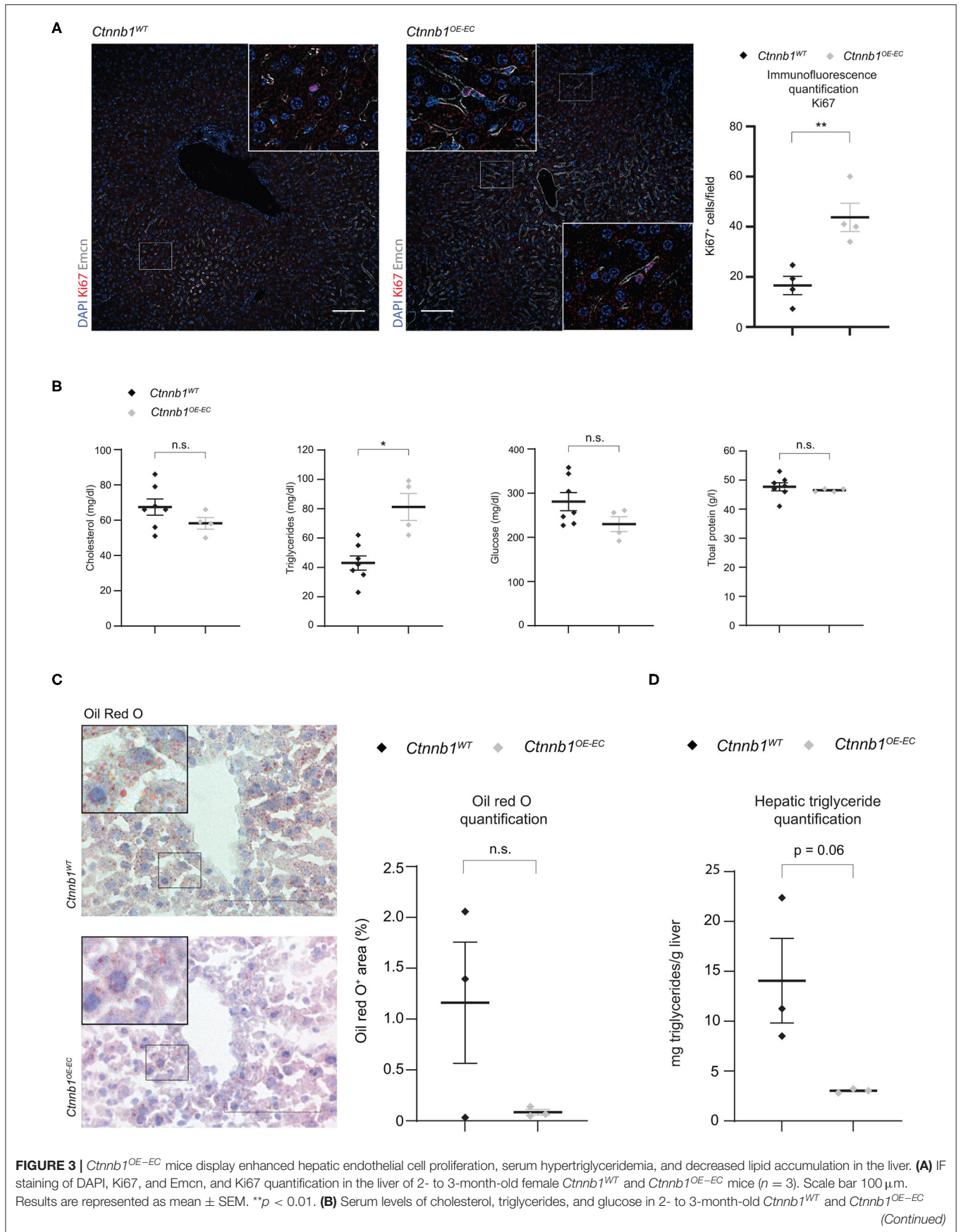
FIGURE 3 | *Ctnnb1^{OE-EC}* mice display enhanced hepatic endothelial cell proliferation, serum hypertriglyceridemia, and decreased lipid accumulation in the liver. **(A)** IF staining of DAPI, Ki67, and Emcn, and Ki67 quantification in the liver of 2- to 3-month-old female *Ctnnb1^{WT}* and *Ctnnb1^{OE-EC}* mice ($n = 3$). Scale bar 100 μm. Results are represented as mean ± SEM. **$p < 0.01$. **(B)** Serum levels of cholesterol, triglycerides, and glucose in 2- to 3-month-old *Ctnnb1^{WT}* and *Ctnnb1^{OE-EC}*

(Continued)

with MX700 transducer, Visualsonics, Toronto, Canada) in parasternal long-axis B- & M-mode, and measured post-processing, which comprised heart rate, left ventricle (LV) posterior and anterior wall thickness, and LV internal diameter at both end-systole and end-diastole. From that, LV volume, LV ejection fraction, and cardiac output were calculated with the Vevo Workstation 5.5.0 and the integrated cardiac measurement package.

Statistics

Statistical analysis was performed with SigmaPlot 11 Software (Systat Software GmbH, Germany). For pairwise comparisons, the *t*-test was used when normality was proved. Differences between data sets with $p < 0.05$ were considered statistically significant. Data are presented as means with error bars indicating standard error.

RESULTS

Generation and Characterization of Adult β-Catenin-Overactivated HEC Mice

EC subtype-specific *Clec4g-iCre* mice (Wohlfeil et al., 2019) were used to generate mice with Ctnnb1 GOF in LSECs (**Figure 1A**). $Ctnnb1^{OE-EC}$ (*Clec4g-iCre$^{tg/wt}$;Ctnnb1(Ex3)$^{fl/wt}$*) mice were viable but were born at a lower Mendelian frequency than expected (**Figure 1B**) and suffered from a reduced overall survival rate (**Figure 1C**). While bodyweight was not altered, heart weight as well as heart weight/body weight ratio were significantly increased in $Ctnnb1^{OE-EC}$ mice (**Figures 1D,E**). As Cre-activity was previously described in ECs of the heart in *Clec4g-iCre* mice (Wohlfeil et al., 2019), a comprehensive analysis of *Clec4g-iCre;R26YFP* reporter mice was performed for this organ. Reporter activity was present in CD31$^+$ ECs of the heart (**Supplementary Figure 1A**). Specifically, YFP positivity was observed in the endocardium, including endomucin (Emcn)$^+$ endocardial trabeculae (Rhee et al., 2018) as well as in CD31$^+$ αSMA$^+$ coronary veins and arteries (Zhang et al., 2005) (**Supplementary Figures 1A,B**). In contrast, LYVE1$^+$ lymphatic vessels were YFP negative (**Supplementary Figure 1B**). In $Ctnnb1^{OE-EC}$ mice, echocardiography revealed progressive cardiac dysfunction, which is comparable to the phenotype obtained after β-catenin GOF mutation in arterial ECs of the heart by using *Bmx-CreER^{T2}* transgenic mice (Nakagawa et al., 2016). $Ctnnb1^{OE-EC}$ mice displayed increased end-diastolic left ventricle internal diameters and volumes (**Figure 1F; Supplementary Figure 2A**) and a reduction in wall thickness of the left ventricle (**Supplementary Figures 2B,C**). The ejection fraction was significantly reduced starting with 2 weeks of age (**Figure 1G**), whereas the cardiac output was first reduced starting with 4 weeks of age (**Supplementary Figure 2D**). A routine histochemical staining of internal organs such as

the kidneys, lungs, spleen, brain, and intestine were gross morphologically unremarkable (**Supplementary Figure 3**).

Endothelial β-catenin overactivation in the liver was confirmed by quantitative reverse-transcription PCR (qRT-PCR), which showed significantly elevated expression of Wnt-/β-catenin downstream target gene axis inhibition protein 2 (*Axin2*) in isolated LSECs from $Ctnnb1^{OE-EC}$ mice (**Figure 2A**). Liver size, liver weight, and liver/body weight ratio were not significantly altered in $Ctnnb1^{OE-EC}$ mice (**Figures 2B,C**). Basic liver function tests did not show elevated levels of ALT, AST, and GLDH (**Figure 2D**). Upon Sirius red staining, no signs of fibrosis were present in the $Ctnnb1^{OE-EC}$ livers (**Figure 2E**). In line with the absence of collagen deposition upon Sirius red staining, no changes in perisinusoidal collagen I, III, or basement membrane collagen IV deposition were seen (**Supplementary Figure 4A**). Additionally, no obvious alterations were seen in livers of $Ctnnb1^{OE-EC}$ mice upon H&E histology, PAS, and Prussian blue staining (**Supplementary Figure 4B**). Likewise, Kupffer cells or hepatic stellate cells (HSC) were not altered in quantity, as analyzed by IF for CD68 or Desmin, respectively (**Figure 2F**). Co-IF of marker proteins for metabolic liver zonation revealed no changes in zonated expression of Glul/GS and Cyp2E1 in pericentral or Arg1 in periportal and midlobular hepatocytes (**Figure 2G; Supplementary Figure 4C**). Notably, there was a significant increase in the Ki67-positivity in ECs from $Ctnnb1^{OE-EC}$ livers, while the proliferation of hepatocytes did not show changes (**Figure 3A**).

Recently, we could demonstrate that EC-derived Wnt signaling controls metabolic liver zonation and alters lipid metabolism (Leibing et al., 2018). Although metabolic liver zonation was not affected by β-catenin GOF mutation, we performed a comprehensive metabolic screening including serum parameters such as total protein, cholesterol, triglycerides, and glucose (**Figure 3B**). Interestingly, $Ctnnb1^{OE-EC}$ mice showed significantly increased serum levels of triglycerides (**Figure 3B**). Liver tissue of $Ctnnb1^{OE-EC}$ mice showed slightly reduced lipid storage upon Oil Red O staining (**Figure 3C**) and a tendency of decreased levels of hepatic triglycerides as measured by a colorimetric assay (**Figure 3D**).

Hepatic Endothelial β-Catenin GOF Mutation Causes Molecular Transdifferentiation of LSECs

To identify β-catenin-dependent molecular alterations in LSECs, we performed comprehensive Affymetrix DNA microarray gene expression profiling of isolated primary LSECs from $Ctnnb1^{WT}$ control and $Ctnnb1^{OE-EC}$ animals. β-catenin GOF mutation in LSECs resulted in the significant dysregulation of 128 genes as compared to control LSECs (**Table 1**). GSEA of LSECs isolated from $Ctnnb1^{WT}$ control and $Ctnnb1^{OE-EC}$ animals revealed significant pathway alterations

TABLE 1 | Differentially expressed genes (DEGs) in $Ctnnb1^{OE-EC}$-LSECs compared to wild-type controls.

Gene symbol	Gene title	Fold change $Ctnnb1^{OE-EC} > Ctnnb1^{WT}$	Adjusted p-value for Diff of genotype = $Ctnnb1^{OE-EC}$–$Ctnnb1^{WT}$
Slc35f2	Solute carrier family 35, member F2	35.13809	0.000397
Apln	Apelin	10.30015045	0.016367
Susd4	Sushi domain containing 4	9.257366289	0.007219
Csf2rb2	Colony stimulating factor 2 receptor, beta 2, low-affinity (granulocyte-macrophage)	8.781086232	0.041067
Cd34	CD34 antigen	8.598926088	0.001273
Selp	Selectin, platelet	8.373297581	0.037503
Lypd6	LY6/PLAUR domain containing 6	8.152209698	0.004191
Glp1r	Glucagon-like peptide 1 receptor	7.081854471	0.041067
Myo1b	Myosin IB	6.942870328	0.023473
St8sia2	ST8 alpha-N-acetyl-neuraminide alpha-2,8-sialyltransferase 2	5.709992179	0.022697
Hunk	Hormonally upregulated Neu-associated kinase	5.184396379	0.045899
St8sia4	ST8 alpha-N-acetyl-neuraminide alpha-2,8-sialyltransferase 4	4.998737335	0.0049
Atp10a	ATPase, class V, type 10A	4.856467229	0.012795
Tcf7	Transcription factor 7, T cell specific	4.800597937	0.013887
Mal	Myelin and lymphocyte protein, T cell differentiation protein	4.715053595	0.025665
Ptgis	Prostaglandin I2 (prostacyclin) synthase	4.52969164	0.030765
Fkbp10	FK506 binding protein 10	4.43037992	0.039368
Axin2	Axin 2	4.416998695	0.022697
Pla2g16	Phospholipase A2, group XVI	4.319974957	0.039368
Il17ra	Interleukin 17 receptor A	3.86500417	0.031256
Disp1	Dispatched RND transporter family member 1	3.826121183	0.031256
Ptgfrn	Prostaglandin F2 receptor negative regulator	3.663983702	0.023473
Greb1l	Growth regulation by estrogen in breast cancer-like	3.513247405	0.0049
Sptb	Spectrin beta, erythrocytic	3.406728181	0.016367
Aqp11	Aquaporin 11	3.384139553	0.026891
Extl3	Exostoses (multiple)-like 3	3.381491933	0.037503
Cttnbp2	Cortactin binding protein 2	3.165960888	0.022697
Kif21b	Kinesin family member 21B	3.103400943	0.002999
Fam213a	Family with sequence similarity 213, member A	3.092980639	0.024278
Auts2	Autism susceptibility candidate 2	3.014691756	0.046838
Tspan6	Tetraspanin 6	2.872077594	0.046282
Lrig1	Leucine-rich repeats and immunoglobulin-like domains 1	2.738931683	0.046282
Pi16	Peptidase inhibitor 16	2.427155192	0.037503
Laptm4b	Lysosomal-associated protein transmembrane 4B	2.318212303	0.011483
Slc7a6	Solute carrier family 7 (cationic amino acid transporter, y+ system), member 6	2.267050692	0.024407
Ptprg	Protein tyrosine phosphatase, receptor type, G	2.158891183	0.022697
Cachd1	Cache domain containing 1	2.065569075	0.007219
Rasgrp4	RAS guanyl releasing protein 4	2.057762756	0.045899
Klhl29	Kelch-like 29	2.027131525	0.036831
Bambi	BMP and activin membrane-bound inhibitor	2.016141198	0.044925
Mlec	Malectin	2.003811198	0.022697
Ppp1r9a	Protein phosphatase 1, regulatory (inhibitor) subunit 9A	1.948922878	0.036956
1810058I24Rik	RIKEN cDNA 1810058I24 gene	1.899752884	0.038628
Osbp2	Oxysterol binding protein 2	1.86993046	0.024407
Gm13889	Predicted gene 13889	1.808734268	0.036956
Vim	Vimentin	1.808581233	0.041067
Gnai1	Guanine nucleotide binding protein (G protein), alpha inhibiting 1	1.795430532	0.036831
Slc1a4	Solute carrier family 1 (glutamate/neutral amino acid transporter), member 4	1.731445442	0.042161

(Continued)

TABLE 1 | Continued

Gene symbol	Gene title	Fold change $Ctnnb1^{OE-EC} > Ctnnb1^{WT}$	Adjusted p-value for Diff of genotype = $Ctnnb1^{OE-EC}-Ctnnb1^{WT}$
Cdc14a	CDC14 cell division cycle 14A	1.727805031	0.041067
Fbl	Fibrillarin	1.67657139	0.045899
Lmo2	LIM domain only 2	1.650427031	0.043595
1110051M20Rik	RIKEN cDNA 1110051M20 gene	1.601538653	0.036831
Cpt1c	Carnitine palmitoyltransferase 1c	1.577681949	0.042456
Fxyd5	FXYD domain-containing ion transport regulator 5	1.552882564	0.038628
Lrrc75a	Leucine rich repeat containing 75A	1.496322239	0.046203
Pgap1	Post-GPI attachment to proteins 1	1.490320435	0.046282
Zfp36l1	Zinc finger protein 36, C3H type-like 1	1.474391469	0.037651
Mir3092	microRNA 3092	1.440648261	0.03784
Ppic	Peptidylprolyl isomerase C	1.435613585	0.043595
Ppdpf	Pancreatic progenitor cell differentiation and proliferation factor	1.336327784	0.041067
Cdk4	Cyclin-dependent kinase 4	1.32815528	0.037503
St3gal4	ST3 beta-galactoside alpha-2,3-sialyltransferase 4	1.281026042	0.036831
D630024D03Rik	RIKEN cDNA D630024D03 gene	1.238041514	0.037503
Cdc45	Cell division cycle 45	1.230144783	0.022697
Eif4g1	Eukaryotic translation initiation factor 4, gamma 1	1.143713408	0.043595
Atp6v1d	ATPase, H+ transporting, lysosomal V1 subunit D	0.893603982	0.048858
Tmx3	Thioredoxin-related transmembrane protein 3	0.84721687	0.048858
Olfr1033	Olfactory receptor 1033	0.83993199	0.042103
Ergic2	ERGIC and golgi 2	0.834146565	0.024407
Aqp1	Aquaporin 1	0.828501756	0.046731
Glra2	Glycine receptor, alpha 2 subunit	0.817240036	0.031256
Gm26744	Predicted gene, 26744	0.810903036	0.046282
Spag9	Sperm associated antigen 9	0.802558367	0.036831
Rnf115	Ring finger protein 115	0.80194744	0.036831
Cd47	CD47 antigen (Rh-related antigen, integrin-associated signal transducer)	0.800896378	0.031314
Dpp4	Dipeptidylpeptidase 4	0.794955116	0.041067
Crebl2	cAMP responsive element binding protein-like 2	0.788857661	0.022697
Atp6ap2	ATPase, H+ transporting, lysosomal accessory protein 2	0.782409663	0.024407
Zfp763	Zinc finger protein 763	0.779090085	0.007745
Fez2	Fasciculation and elongation protein zeta 2 (zygin II)	0.762992727	0.036831
Zfp715	Zinc finger protein 715	0.744750505	0.048858
Cyb561d1	Cytochrome b-561 domain containing 1	0.744262296	0.048858
Extl2	Exostoses (multiple)-like 2	0.728699546	0.048068
Golga7	Golgi autoantigen, golgin subfamily a, 7	0.723018512	0.026891
Tgoln1	Trans-golgi network protein	0.721857092	0.036831
Tpm3	Tropomyosin 3, gamma	0.717139012	0.044415
Ggh	Gamma-glutamyl hydrolase	0.714504325	0.048882
Scrn3	Secernin 3	0.707136697	0.046282
Irak2	Interleukin-1 receptor-associated kinase 2	0.68925238	0.037503
Tmem170b	Transmembrane protein 170B	0.685022667	0.046847
Dgke	Diacylglycerol kinase, epsilon	0.681193453	0.024407
Itga1	Integrin alpha 1	0.676125877	0.041067
Sdccag8	Serologically defined colon cancer antigen 8	0.662856645	0.041067
Hspa12a	Heat shock protein 12A	0.647460358	0.046907
Nceh1	Neutral cholesterol ester hydrolase 1	0.641787883	0.042161
Impact	Impact, RWD domain protein	0.641068766	0.022697
Nlrc3	NLR family, CARD domain containing 3	0.616870496	0.024407
Pitpnm1	Phosphatidylinositol transfer protein, membrane-associated 1	0.607880798	0.024407

(Continued)

TABLE 1 | Continued

Gene symbol	Gene title	Fold change $Ctnnb1^{OE-EC} > Ctnnb1^{WT}$	Adjusted p-value for Diff of genotype = $Ctnnb1^{OE-EC}–Ctnnb1^{WT}$
Gm19663	Predicted gene, 19663	0.601230962	0.035201
Inpp4b	Inositol polyphosphate-4-phosphatase, type II	0.598629428	0.048227
Pde3b	Phosphodiesterase 3B, cGMP-inhibited	0.586483967	0.036956
P2ry10b	Purinergic receptor P2Y, G-protein coupled 10B	0.58265069	0.044415
Ldhb	Lactate dehydrogenase B	0.575509392	0.031256
Smco4	Single-pass membrane protein with coiled-coil domains 4	0.546281346	0.039368
Gm14005	Predicted gene 14005	0.545796227	0.046282
A630072L19Rik	RIKEN cDNA A630072L19 gene	0.545449977	0.037503
Cyp7b1	Cytochrome P450, family 7, subfamily b, polypeptide 1	0.537648924	0.039821
Ldb2	LIM domain binding 2	0.526662693	0.036831
Nudt12	Nudix (nucleoside diphosphate linked moiety X)-type motif 12	0.522324687	0.037503
Cfh	Complement component factor h	0.521077661	0.036831
Ptpru	Protein tyrosine phosphatase, receptor type, U	0.517441974	0.042879
Pgghg	Protein glucosylgalactosylhydroxylysine glucosidase	0.479186666	0.048882
Acer3	Alkaline ceramidase 3	0.472763137	0.036831
Ceacam1	Carcinoembryonic antigen-related cell adhesion molecule 1	0.472603157	0.041067
Ccdc88c	Coiled-coil domain containing 88C	0.469087339	0.027307
Fam189a2	Family with sequence similarity 189, member A2	0.467888229	0.041067
Cysltr2	Cysteinyl leukotriene receptor 2	0.442737637	0.023473
Gramd1c	GRAM domain containing 1C	0.42091094	0.004191
Ntf3	Neurotrophin 3	0.420199255	0.038876
Fam174b	Family with sequence similarity 174, member B	0.414689246	0.037572
Slc26a10	Solute carrier family 26, member 10	0.394412144	0.022697
Pla2r1	Phospholipase A2 receptor 1	0.354842083	0.048858
Gpc1	Glypican 1	0.354767031	0.022697
Rnase4	Ribonuclease, RNase A family 4	0.321464634	0.043595
Olfm1	Olfactomedin 1	0.276916317	0.036956
Cd209b	CD209b antigen	0.268887021	0.009718
Flrt1	Fibronectin leucine rich transmembrane protein 1	0.200652325	0.048858
Ada	Adenosine deaminase	0.153417209	0.022697

Genes are displayed that were significantly up- or downregulated when compared to Ctnnb1^{WT} controls with Fold change (FC) < 1 or > 1. Adjusted p-values were calculated for the differences of means of log10 of expression values between Ctnnb1^{OE-EC} and Ctnnb1^{WT}.

in the Hallmark gene sets. Among the most regulated gene sets, we found "Myc targets V1 and V2" and "Cholesterol homeostasis" (**Figure 4A**) followed by "G2M Checkpoint" and "E2F targets." Furthermore, GSEA confirmed the activation of Wnt/β-catenin signaling in β-catenin GOF mutation in LSECs (**Figure 4A**). Overrepresentation analysis (ORA) of the significantly dysregulated genes by using Enrichr revealed significant alterations in the gene ontology (GO) biological processes 2018 library (**Figure 4B**). "Positive regulation of cell differentiation" was identified as the most significant GO term in LSECs with β-catenin GOF mutation (**Figure 4B**).

An established panel of LSEC-associated and CEC-associated marker genes (Geraud et al., 2010, 2017; Olsavszky et al., 2020) was analyzed in LSECs isolated from *Ctnnb1^{WT}* control and *Ctnnb1^{OE-EC}* animals. Gene expression analysis pointed out that β-catenin GOF mutation in LSECs of *Ctnnb1^{OE-EC}*

mice dysregulated LSEC- and CEC-associated genes (**Figure 4C**). GSEA revealed a significant induction of a CEC-associated gene set (**Figure 4D**) and a significant loss of an LSEC gene set (**Figure 4E**). As Wnt-/β-catenin signaling is a well-known driver for brain endothelial differentiation (Liebner et al., 2008), we hypothesized that β-catenin signaling activation in LSECs might result in partial brain EC reprograming. When performing GSEA with a brain endothelial gene set, which was generated by comparing published single-cell RNA-seq data from brain vs. liver ECs (Sabbagh et al., 2018), a significant enrichment for brain EC transcripts was found in *Ctnnb1^{OE-EC}* LSEC (**Figure 4F**). Among the genes that were significantly upregulated in *Ctnnb1^{OE-EC}* LSEC with a fold-change of >2, several genes could be detected that were also highly expressed in brain ECs (**Table 2**). As the expression of TJ molecule, Cldn5 was previously shown to be upregulated by endothelial Wnt-/β-catenin GOF in the leaky suprafornical organ (Benz et al., 2019), we compared
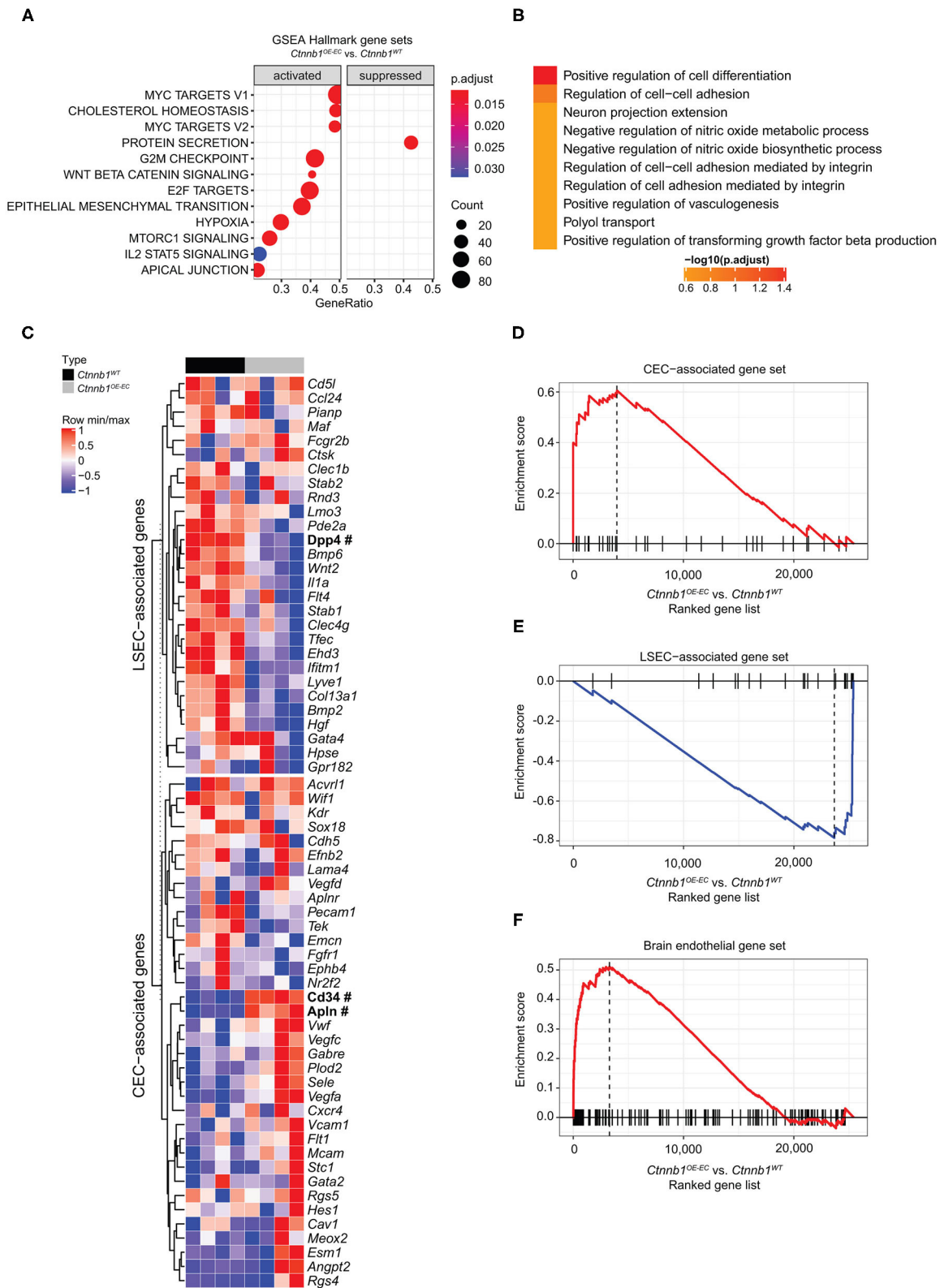
FIGURE 4 | Hepatic endothelial *Ctnnb1* overactivation causes sinusoidal transdifferentiation. **(A)** Gene Set Enrichment Analysis-Kyoto Encyclopedia of Genes and Genomes (GSEA-KEGG) pathway alterations analyzed using MSigDB hallmark gene sets in freshly isolated LSECs from 2-month-old female *Ctnnb1*[WT] and *Ctnnb1*[OE−EC] (*n* = 4). **(B)** Overrepresentation analysis of gene ontology "biological processes" library. **(C)** Heat map of the liver sinusoidal endothelial cell (LSEC)- and

(Continued)

FIGURE 4 | continuous endothelial cell (CEC)-associated genes. Selected genes are shown for isolated LSECs from $Ctnnb1^{WT}$ (black) and $Ctnnb1^{OE-EC}$ mice (gray). Significant samples are written in bold and marked with # (n = 4 samples per group). The heat map color represents the mean and maximum values for each gene. The intensity scale of the standardized expression values ranges from dark blue (low expression) to dark red (high expression). Enrichment plots of **(D)** LSEC-associated (p = 0.0023; NES = −2.43) and **(E)** CEC-associated (p = 0.0023; NES = 2.04) genes (n = 4). **(F)** Enrichment plots of brain endothelial genes (p = 0.0001; NES = 2.16) (n = 4).

TABLE 2 | Brain endothelial transcripts.

Gene symbol	Gene title	Fold change $Ctnnb1^{OE-EC} > Ctnnb1^{WT}$	Adjusted p-value for Diff of genotype = $Ctnnb1^{OE-EC} - Ctnnb1^{WT}$
Slc35f2	Solute carrier family 35, member F2	35.13809	0.000397
Myo1b	Myosin IB	6.942870328	0.023473
Tcf7	Transcription factor 7, T cell specific	4.800597937	0.013887
Axin2	Axin 2	4.416998695	0.022697
Pla2g16	Phospholipase A2, group XVI	4.319974957	0.039368
Il17ra	Interleukin 17 receptor A	3.86500417	0.031256
Extl3	Exostoses (multiple)-like 3	3.381491933	0.037503
Ptprg	Protein tyrosine phosphatase, receptor type, G	2.158891183	0.022697
Cachd1	Cache domain containing 1	2.065569075	0.007219

Genes are displayed that were significantly upregulated in $Ctnnb1^{OE-EC}$ LSEC compared to $Ctnnb1^{WT}$ LSEC with a fold change (FC) > 2 and also overexpressed in brain endothelial cells compared to liver endothelial cells (Daneman et al., 2010; Sabbagh et al., 2018).

the expression levels of Cldn5 in $Ctnnb1^{OE-EC}$ and control liver. Expression of Cldn5 was not altered in $Ctnnb1^{OE-EC}$ compared with control LSECs (**Supplementary Figure 5A**).

In addition, the expression of markers for endothelial zonation, that is, Emcn and LYVE1 (Walter et al., 2014) were analyzed. A significant loss of mid-zonal LSEC marker LYVE1 was found, indicating disturbed endothelial liver zonation (**Figures 5A,B**). However, the expression of pericentral LSEC and CEC marker Emcn was not altered on protein level (**Figure 5A**). Despite disturbed endothelial zonation, the expression of pan-endothelial marker podocalyxin or CD31 was unaltered indicating no major changes in vascular density in $Ctnnb1^{OE-EC}$ livers (**Supplementary Figure 5B**). Furthermore, β-catenin GOF in the LSECs did not alter the expression of LSEC marker CD32b (**Supplementary Figure 5C**), LSEC scavenger receptors *Stab1* and *Stab2* (**Supplementary Figures 5D,E**) or CEC markers *Vegfr2*, Caveolin-1, ICAM1, vascular cell adhesion molecule (VCAM), or VE-cadherin (**Supplementary Figures 5C, 6A–C**).

To confirm the transcriptomic alterations seen in $Ctnnb1^{OE-EC}$ LSEC, we performed immunofluorescent staining, real-time quantitative PCR (qRT-PCR), and ISH for selected EC genes and proteins. The selection was either based on significant regulation among the list of CEC-associated genes (**Figure 4C**), relation to liver fibrosis [Gata4, Myc, platelet-derived growth factor subunit B (*Pdgfb*)] (Winkler et al., 2021), or established LSEC angiocrine factors. Upon ISH, the expression of the bone morphogenetic protein (*Bmp*) 2 was not significantly altered (**Figures 5C,D**). This was in line with Prussian blue staining of the liver, which did not show iron deposition in the liver of $Ctnnb1^{OE-EC}$ mice (**Supplementary Figure 4B**). Moreover, *Hamp* expression in liver lysates was unaltered, indicating preserved BMP2–HAMP

signaling (**Supplementary Figure 4D**). While LSEC angiocrine factor *Wnt2* was significantly downregulated, *Hgf* and *Wnt9b* were not significantly altered (**Figures 5C,D**). β-catenin GOF mutation in LSECs did not alter the expression of LSEC master regulator GATA4 on protein or mRNA level (**Figure 5E**) or pro-fibrotic angiocrine factor *Pdgfb* (**Figure 5F**). On the contrary, transcription factor *Myc* and CEC markers *CD34* and *Apln* were significantly upregulated in $Ctnnb1^{OE-EC}$ LSEC (**Figures 4C**, **5F–H**).

DISCUSSION

Our data show that imbalanced or overactivated β-catenin signaling in LSECs leads to sinusoidal transdifferentiation, including dysregulated lipid homeostasis. Reduced overall survival of $Ctnnb1^{OE-EC}$ mice was most likely independent from LSEC transdifferentiation and dysregulated lipid homeostasis, but rather resulted from progressive heart dysfunction. The heart phenotype observed in $Ctnnb1^{OE-EC}$ mice is comparable to β-catenin GOF mutation studies in arterial ECs by using a *Bmx-CreER*[T2] mice, although reporter activity in heart ECs of *Clec4g-iCre;R26YFP* mice was identified in more than just arterial ECs, namely in heart capillaries, endocardium, and venous coronary vessels. Mechanistically, activation of Wnt-/β-catenin signaling in arterial ECs of the heart was shown to result in progressive heart failure through suppressing neuregulin-ErbB signaling (Nakagawa et al., 2016).

In the liver, β-catenin GOF mutation in LSECs resulted in sinusoidal-to-continuous transdifferentiation with downregulation of midzonal LSEC marker LYVE1 and angiocrine factor *Wnt2*, and upregulation of CEC markers *CD34* and *Apln*. This rather "mild" capillarization program lacking HSC activation and perisinusoidal extracellular matrix
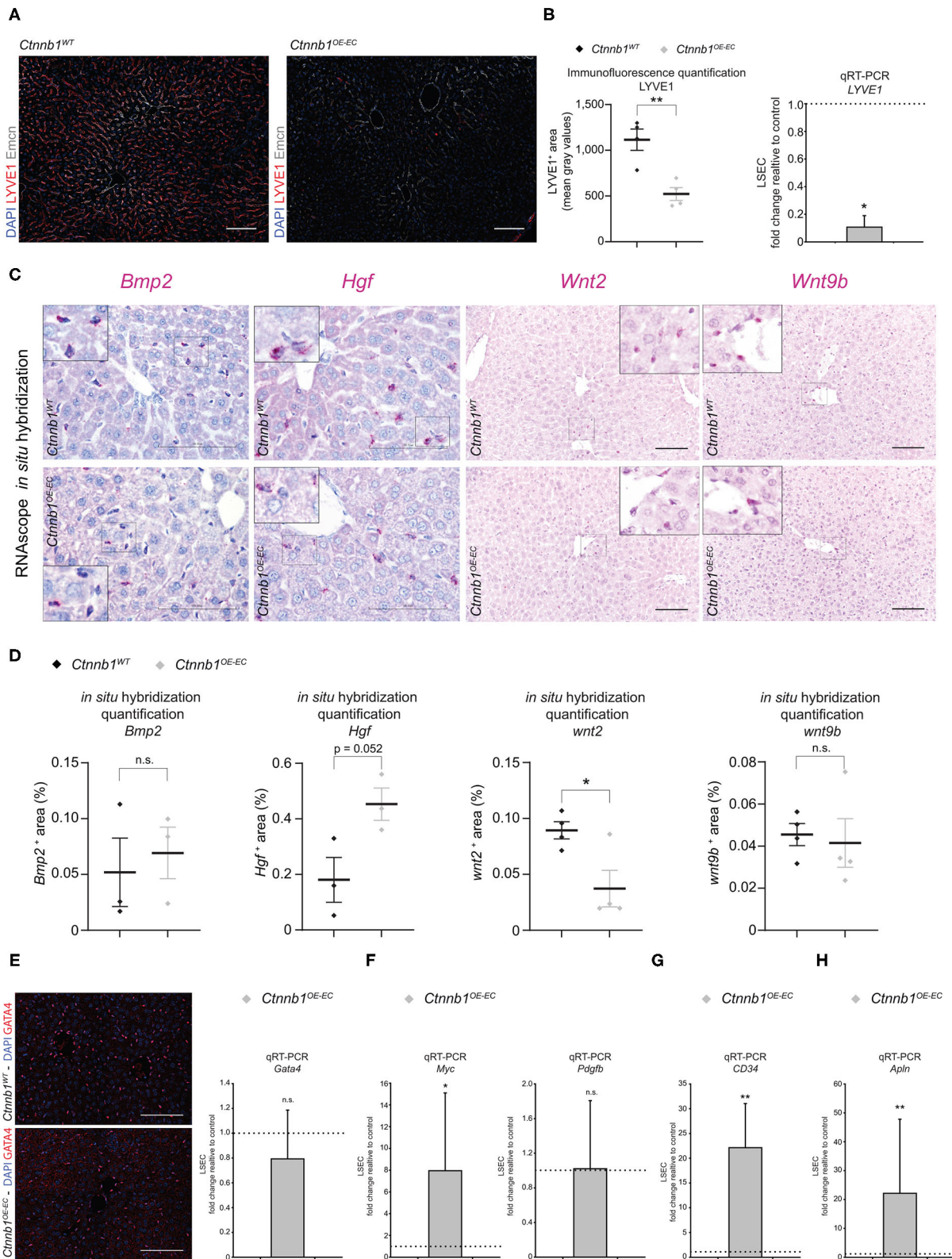
FIGURE 5 | Hepatic endothelial *Ctnnb1* overactivation causes loss of LSEC-associated genes and induction of CEC and brain EC genes. **(A)** IF staining of DAPI, LYVE1, and Emcn in the liver of 2- to 3-month-old female *Ctnnb1^WT* and *Ctnnb1^OE−EC* mice (*n* = 4). Scale bar 100 μm. **(B)** Left panel: IF quantification of LYVE1+ area. Results are represented as mean ± SEM. **p < 0.01. Right panel: qRT-PCR for *LYVE1* of cDNA from *Ctnnb1^OE−EC*-LSECs compared to *Ctnnb1^WT* control

(Continued)

deposition did not result in hepatopathy or liver fibrosis. Interestingly, Wnt-target gene *Myc* (He et al., 1998) was significantly induced in *Ctnnb1^{OE-EC}* LSECs. Previous work by us could show, that loss of LSEC master regulator GATA4 also induced pro-angiogenic *Myc* in LSECs, to further amplify a pro-fibrotic angiocrine program, including *de novo Pdgfb* expression, resulting in perisinusoidal liver fibrosis (Winkler et al., 2021). β-catenin GOF in LSECs did not significantly regulate GATA4 expression, which most likely protects against a complete capillarization program and perisinusoidal liver fibrosis by suppressing pro-fibrotic angiocrine factors such as *Pdgfb*, which was unaltered in *Ctnnb1^{OE-EC}* LSEC despite a significant *Myc* induction.

Angiocrine Wnt-signaling is vital for liver growth and metabolic liver zonation and Wnt-signaling in LSECs is linked to autocrine growth effects (Klein et al., 2008; Geraud et al., 2010; Leibing et al., 2018). While activation of β-catenin in LSECs reduced angiocrine *Wnt2*, this reduction together with unaltered *Wnt9b* was not sufficient to impair metabolic liver zonation in *Ctnnb1^{OE-EC}* mice. Interestingly, EC proliferation was significantly induced by activation of β-catenin in LSECs. These findings are supported by GSEA results of *Ctnnb1^{OE-EC}* LSEC with enrichment in the gene sets "G2M Checkpoint" and "E2F Targets," both resembling a pro-proliferative state, thereby indicating that β-catenin overactivation in LSECs stimulates endothelial proliferation. This is in line with data observed in postnatal brain and retina, showing that deficiency of endothelial β-catenin signaling impairs endothelial proliferation and sprouting (Martowicz et al., 2019).

Notably, activation of β-catenin in LSECs resulted in the upregulation of genes that are known to be expressed by the brain ECs (Daneman et al., 2010; Wang et al., 2019) and GSEA could confirm the enrichment of brain EC transcripts (Sabbagh et al., 2018) in *Ctnnb1^{OE-EC}* LSECs. In contrast to LSEC, that belong to discontinuous sinusoidal ECs which enable transfer of fluids, nutrients, and small solutes through open fenestrations within the sinusoidal wall (Wisse et al., 1985; Augustin and Koh, 2017), the brain ECs belong to the group of CECs, expressing specialized TJ molecules and transporters for restricting paracellular passage and transcellular trafficking, thereby generating the tightly sealed blood–brain barrier (Langen et al., 2019). In line with our results, ectopic β-catenin signaling activation in the highly permeable and fenestrated vasculature of the circumventricular organs is sufficient for BBB reprograming (Benz et al., 2019; Wang et al., 2019). Furthermore, inducible pan-endothelial Ctnnb1 GOF showed some overlap with genes dysregulated in *Ctnnb1^{OE-EC}* LSEC despite using

different Cre lines (Munji et al., 2019). Vice-versa, loss of Wnt-signaling activity impairs brain endothelial differentiation by downregulating TJ molecules and transporter proteins, while increasing the expression of the plasmalemma vesicle–associated protein (PLVAP) (Liebner et al., 2008; Stenman et al., 2008; Daneman et al., 2009). However, the expression of TJ molecule Cldn5 was not enhanced in *Ctnnb1^{OE-EC}* LSEC, which could be a result of maintained expression of LSEC master regulator GATA4. Notably, PLVAP knockout mice developed a reduction of LSEC fenestrations, which led to elevated serum levels of triglycerides, low-density lipoprotein, and cholesterol due to retention of chylomicron remnants in the blood. The authors speculated that compensatory hepatocyte *de novo* lipogenesis was responsible for steatosis, steatohepatitis, and liver fibrosis (Herrnberger et al., 2014). *Ctnnb1^{OE-EC}* mice neither showed liver steatosis nor fibrosis, which argue against reduced PLVAP expression as a main driver of isolated hypertriglyceridemia in *Ctnnb1^{OE-EC}* mice.

As only microvascular ECs in the liver with sinusoidal differentiation allow filtration of chylomicron remnants from the blood (Fraser et al., 1995; Cogger et al., 2006), β-catenin-mediated transdifferentiation of liver sinusoids with partial BBB reprograming in *Ctnnb1^{OE-EC}* mice may impair uptake of chylomicrons and subsequently lead to elevated serum lipid levels. However, these metabolic alterations are in contrast with previous results, showing that neither sinusoidal capillarization with loss of fenestrations and formation of a basement membrane in Gata4-deficient LSEC (*Gata4$^{LSEC-KO}$*), nor partial sinusoidal capillarization/trandifferentiation in mice with enhanced Notch signaling in LSECs (*NICD^{OE-HEC}*) are associated with reduced levels of serum cholesterol and triglycerides (Wohlfeil et al., 2019; Winkler et al., 2021). This argues against a general impairment of lipid transfer into the space of Disse during sinusoidal capillarization/transdifferentiation and indicates that hypertriglyceridemia in *Ctnnb1^{OE-EC}* mice is a result of β-catenin-mediated LSEC transdifferentiation by impaired transendothelial transport mechanisms and/or by altered angiocrine signaling that control hepatocyte lipogenesis/lipolysis.

Among the *de novo* expressed genes in *Ctnnb1^{OE-EC}* LSEC, *Apln* was found as the second most upregulated gene. Apelin (APLN) is a secreted peptide, which is widely expressed in different cell types, including CECs and is also known as a regulator of transendothelial lipid transport (Hwangbo et al., 2017). Mice with *Apln* knockout become obese and show more fat deposition as a consequence of increased vascular permeability with greater uptake of fatty acids. On the other hand, transgenic *Apln* mice that express apelin under the

transcriptional control of the keratin 14 promoter are protected from obesity and show a reduced endothelial permeability (Sawane et al., 2011, 2013). Interestingly, Huang and colleagues were able to show that also Apln signaling in hepatocytes protects against lipid accumulation in the liver (Huang et al., 2017). As the promoter region of the *Apln* gene has transcription factor–binding sites for Wnt signaling downstream targets *Tcf/Lef* (Chen et al., 2019), *Apln* expression might be transcriptionally activated by Wnt-β-catenin signaling activation in $Ctnnb1^{OE-EC}$ LSECs. This is in line with silencing experiments of β-catenin in pulmonary ECs showing that *Apln* mRNA and protein expression were reduced (Alastalo et al., 2011). Thus, in $Ctnnb1^{OE-EC}$ mice de novo *Apln* expression in transdifferentiated LSECs may be involved in dysregulated lipid homeostasis. Yet, one has to consider that aberrant *Apln* expression is also found in $CD34^+$ capillarized LSECs in liver fibrosis (Winkler et al., 2021) and cirrhosis (Yokomori et al., 2012) and also pro-angiogenic effects were similar to the vascular apelin signaling (Helker et al., 2020).

Together, normal sinusoidal differentiation is decisive for the fulfillment of the typical LSEC functions such as scavenging, immunoregulation, protection against stellate cell activation, and fibrosis, but also for the angiocrine regulation of liver regeneration and iron metabolism (Poisson et al., 2017; Shetty et al., 2018; Lafoz et al., 2020; Koch et al., 2021). While endothelial Wnt-signaling activity is largely confined to brain ECs for the maintenance of the BBB (Sabbagh et al., 2018), here we can show for the first time that low-level liver endothelial Wnt-signaling *in vivo* is crucial for maintaining sinusoidal differentiation, which is required for regulation of proper hepatic lipid metabolism. Further research is necessary to analyze the specific contributions of LSECs in hepatic fat absorption and metabolism. Future work will have to address which angiocrine signaling pathways may be involved in this process, extending the knowledge that liver endothelial fatty acid absorption is not mainly a passive mechanism mediated by open fenestrations in LSECs. This is of particular interest as dyslipidemia is a major risk factor for cardiovascular disease.

DATA AVAILABILITY STATEMENT

The datasets presented in this study can be found in online repositories. The names of the repository/repositories and accession number(s) can be found at: https://www.ncbi.nlm.nih.gov/geo/query/acc.cgi?acc=GSE175777.

ETHICS STATEMENT

The animal study was reviewed and approved by Regional Council Karlsruhe. Written informed consent was obtained from the owners for the participation of their animals in this study.

AUTHOR CONTRIBUTIONS

P-SK, KSa, SG, and VO: study concept and design. P-SK, KSa, JHeil, CDS, SK, JHo, MW, CT, CS, KSc, MT, FT, JHein, CG, SG, and VO: experimental work, analysis, and interpretation of data. P-SK, KSa, and VO: writing original draft. All authors writing and reviewing the manuscript before submission.

SUPPLEMENTARY MATERIAL

The Supplementary Material for this article can be found online at: https://www.frontiersin.org/articles/10.3389/fphys.2021.722394/full#supplementary-material

REFERENCES

Alastalo, T. P., Li, M., Perez Vde, J., Pham, D., Sawada, H., Wang, J. K., et al. (2011). Disruption of PPARgamma/beta-catenin-mediated regulation of apelin impairs BMP-induced mouse and human pulmonary arterial EC survival. *J. Clin. Invest.* 121, 3735–3746. doi: 10.1172/JCI 43382

Augustin, H. G., and Koh, G. Y. (2017). Organotypic vasculature: from descriptive heterogeneity to functional pathophysiology. *Science* 357:eaal2379. doi: 10.1126/science.aal2379

Benz, F., Wichitnaowarat, V., Lehmann, M., Germano, R. F., Mihova, D., Macas, J., et al. (2019). Low wnt/beta-catenin signaling determines leaky vessels in the subfornical organ and affects water homeostasis in mice. *Elife* 8:e43818. doi: 10.7554/eLife.43818.044

Cao, Z., Ye, T., Sun, Y., Ji, G., Shido, K., Chen, Y., et al. (2017). Targeting the vascular and perivascular niches as a regenerative therapy for lung and liver fibrosis. *Sci. Transl. Med.* 9:eaai8710. doi: 10.1126/scitranslmed.aai8710

Chen, E. Y., Tan, C. M., Kou, Y., Duan, Q., Wang, Z., Meirelles, G. V., et al. (2013). Enrichr: interactive and collaborative HTML5 gene list enrichment analysis tool. *BMC Bioinformatics* 14:128. doi: 10.1186/1471-2105-14-128

Chen, H., Wong, C. C., Liu, D., Go, M. Y. Y., Wu, B., Peng, S., et al. (2019). APLN promotes hepatocellular carcinoma through activating PI3K/Akt pathway and is a druggable target. *Theranostics* 9, 5246–5260. doi: 10.7150/thno.34713

Choi, H. J., Park, H., Lee, H. W., and Kwon, Y. G. (2012). The Wnt pathway and the roles for its antagonists, DKKS, in angiogenesis. *IUBMB Life* 64, 724–731. doi: 10.1002/iub.1062

Cogger, V. C., Hilmer, S. N., Sullivan, D., Muller, M., Fraser, R., and Le Couteur, D. G. (2006). Hyperlipidemia and surfactants: the liver sieve is a link. *Atherosclerosis* 189, 273–281. doi: 10.1016/j.atherosclerosis.2005.12.025

Corada, M., Nyqvist, D., Orsenigo, F., Caprini, A., Giampietro, C., Taketo, M. M., et al. (2010). The Wnt/beta-catenin pathway modulates vascular remodeling and specification by upregulating Dll4/Notch signaling. *Dev. Cell* 18, 938–949. doi: 10.1016/j.devcel.2010.05.006

Daneman, R., Agalliu, D., Zhou, L., Kuhnert, F., Kuo, C. J., and Barres, B. A. (2009). Wnt/beta-catenin signaling is required for CNS, but not non-CNS, angiogenesis. *Proc. Natl. Acad. Sci. U.S.A.* 106, 641–646. doi: 10.1073/pnas.0805165106

Daneman, R., Zhou, L., Agalliu, D., Cahoy, J. D., Kaushal, A., and Barres, B. A. (2010). The mouse blood-brain barrier transcriptome: a new resource for understanding the development and function of brain endothelial cells. *PLoS ONE* 5:e13741. doi: 10.1371/journal.pone.0013741

Deb, A. (2014). Cell-cell interaction in the heart via Wnt/beta-catenin pathway after cardiac injury. *Cardiovasc. Res.* 102, 214–223. doi: 10.1093/cvr/cvu054

Decaens, T., Godard, C., De Reynies, A., Rickman, D. S., Tronche, F., Couty, J. P., et al. (2008). Stabilization of beta-catenin affects mouse embryonic liver growth and hepatoblast fate. *Hepatology* 47, 247–258. doi: 10.1002/hep.21952

Ding, B. S., Nolan, D. J., Butler, J. M., James, D., Babazadeh, A. O., Rosenwaks, Z., et al. (2010). Inductive angiocrine signals from sinusoidal endothelium are required for liver regeneration. *Nature* 468, 310–315. doi: 10.1038/nature09493

Duarte, A., Hirashima, M., Benedito, R., Trindade, A., Diniz, P., Bekman, E., et al. (2004). Dosage-sensitive requirement for mouse Dll4 in artery development. *Genes Dev.* 18, 2474–2478. doi: 10.1101/gad.1239004

Fraser, R., Dobbs, B. R., and Rogers, G. W. (1995). Lipoproteins and the liver sieve: the role of the fenestrated sinusoidal endothelium in lipoprotein metabolism, atherosclerosis, and cirrhosis. *Hepatology* 21, 863–874. doi: 10.1002/hep.1840210337

Geraud, C., Evdokimov, K., Straub, B. K., Peitsch, W. K., Demory, A., Dorflinger, Y., et al. (2012). Unique cell type-specific junctional complexes in vascular endothelium of human and rat liver sinusoids. *PLoS ONE* 7:e34206. doi: 10.1371/journal.pone.0034206

Geraud, C., Koch, P. S., Zierow, J., Klapproth, K., Busch, K., Olsavszky, V., et al. (2017). GATA4-dependent organ-specific endothelial differentiation controls liver development and embryonic hematopoiesis. *J. Clin. Invest.* 127, 1099–1114. doi: 10.1172/JCI90086

Geraud, C., Schledzewski, K., Demory, A., Klein, D., Kaus, M., Peyre, F., et al. (2010). Liver sinusoidal endothelium: a microenvironment-dependent differentiation program in rat including the novel junctional protein liver endothelial differentiation-associated protein-1. *Hepatology* 52, 313–326. doi: 10.1002/hep.23618

Gu, Z., Eils, R., and Schlesner, M. (2016). Complex heatmaps reveal patterns and correlations in multidimensional genomic data. *Bioinformatics* 32, 2847–2849. doi: 10.1093/bioinformatics/btw313

Harada, N., Tamai, Y., Ishikawa, T., Sauer, B., Takaku, K., Oshima, M., et al. (1999). Intestinal polyposis in mice with a dominant stable mutation of the beta-catenin gene. *EMBO J.* 18, 5931–5942. doi: 10.1093/emboj/18.21.5931

He, T. C., Sparks, A. B., Rago, C., Hermeking, H., Zawel, L., Da Costa, L. T., et al. (1998). Identification of c-MYC as a target of the APC pathway. *Science* 281, 1509–1512. doi: 10.1126/science.281.5382.1509

Helker, C. S., Eberlein, J., Wilhelm, K., Sugino, T., Malchow, J., Schuermann, A., et al. (2020). Apelin signaling drives vascular endothelial cells toward a pro-angiogenic state. *Elife* 9:e55589. doi: 10.7554/eLife.55589.sa2

Herrnberger, L., Hennig, R., Kremer, W., Hellerbrand, C., Goepferich, A., Kalbitzer, H. R., et al. (2014). Formation of fenestrae in murine liver sinusoids depends on plasmalemma vesicle-associated protein and is required for lipoprotein passage. *PLoS ONE* 9:e115005. doi: 10.1371/journal.pone.0115005

Huang, J., Kang, S., Park, S. J., and Im, D. S. (2017). Apelin protects against liver X receptor-mediated steatosis through AMPK and PPARalpha in human and mouse hepatocytes. *Cell. Signal.* 39, 84–94. doi: 10.1016/j.cellsig.2017.08.003

Hwangbo, C., Wu, J., Papangeli, I., Adachi, T., Sharma, B., Park, S., et al. (2017). Endothelial APLNR regulates tissue fatty acid uptake and is essential for apelin's glucose-lowering effects. *Sci. Transl. Med.* 9:eaad4000. doi: 10.1126/scitranslmed.aad4000

Klein, D., Demory, A., Peyre, F., Kroll, J., Augustin, H. G., Helfrich, W., et al. (2008). Wnt2 acts as a cell type-specific, autocrine growth factor in rat hepatic sinusoidal endothelial cells cross-stimulating the VEGF pathway. *Hepatology* 47, 1018–1031. doi: 10.1002/hep.22084

Koch, P.-S., Lee, K. H., Goerdt, S., and Augustin, H. G. (2021). Angiodiversity and organotypic functions of sinusoidal endothelial cells. *Angiogenesis* 24, 289–310. doi: 10.1007/s10456-021-09780-y

Korotkevich, G., Sukhov, V., Budin, N., Shpak, B., Artyomov, M. N., and Sergushichev, A. (2021). Fast gene set enrichment analysis. *bioRxiv [Preprint]* doi: 10.1101/060012

Kostallari, E., and Shah, V. H. (2016). Angiocrine signaling in the hepatic sinusoids in health and disease. *Am. J. Physiol. Gastrointest. Liver Physiol.* 311, G246–G251. doi: 10.1152/ajpgi.00118.2016

Lafoz, E., Ruart, M., Anton, A., Oncins, A., and Hernandez-Gea, V. (2020). The endothelium as a driver of liver fibrosis and regeneration. *Cells* 9:929. doi: 10.3390/cells9040929

Lalor, P. F., Lai, W. K., Curbishley, S. M., Shetty, S., and Adams, D. H. (2006). Human hepatic sinusoidal endothelial cells can be distinguished by expression of phenotypic markers related to their specialised functions *in vivo. World J. Gastroenterol.* 12, 5429–5439. doi: 10.3748/wjg.v12.i34.5429

Langen, U. H., Ayloo, S., and Gu, C. (2019). Development and cell biology of the blood-brain barrier. *Annu. Rev. Cell Dev. Biol.* 35, 591–613. doi: 10.1146/annurev-cellbio-100617-062608

Leibing, T., Geraud, C., Augustin, I., Boutros, M., Augustin, H. G., Okun, J. G., et al. (2018). Angiocrine Wnt signaling controls liver growth and metabolic maturation in mice. *Hepatology* 68, 707–722. doi: 10.1002/hep.29613

Liberzon, A., Birger, C., Thorvaldsdottir, H., Ghandi, M., Mesirov, J. P., and Tamayo, P. (2015). The molecular signatures database (MSigDB) hallmark gene set collection. *Cell Syst.* 1, 417–425. doi: 10.1016/j.cels.2015.12.004

Liebner, S., Corada, M., Bangsow, T., Babbage, J., Taddei, A., Czupalla, C. J., et al. (2008). Wnt/beta-catenin signaling controls development of the blood-brain barrier. *J. Cell Biol.* 183, 409–417. doi: 10.1083/jcb.200806024

Martowicz, A., Trusohamn, M., Jensen, N., Wisniewska-Kruk, J., Corada, M., Ning, F. C., et al. (2019). Endothelial beta-Catenin signaling supports postnatal brain and retinal angiogenesis by promoting sprouting, tip cell formation, and VEGFR (vascular endothelial growth factor receptor) 2 expression. *Arterioscler Thromb. Vasc. Biol.* 39, 2273–2288. doi: 10.1161/ATVBAHA.119.312749

Masckauchan, T. N., Shawber, C. J., Funahashi, Y., Li, C. M., and Kitajewski, J. (2005). Wnt/beta-catenin signaling induces proliferation, survival and interleukin-8 in human endothelial cells. *Angiogenesis* 8, 43–51. doi: 10.1007/s10456-005-5612-9

Munji, R. N., Soung, A. L., Weiner, G. A., Sohet, F., Semple, B. D., Trivedi, A., et al. (2019). Profiling the mouse brain endothelial transcriptome in health and disease models reveals a core blood-brain barrier dysfunction module. *Nat. Neurosci.* 22, 1892–1902. doi: 10.1038/s41593-019-0497-x

Nakagawa, A., Naito, A. T., Sumida, T., Nomura, S., Shibamoto, M., Higo, T., et al. (2016). Activation of endothelial beta-catenin signaling induces heart failure. *Sci. Rep.* 6:25009. doi: 10.1038/srep25009

Nolan, D. J., Ginsberg, M., Israely, E., Palikuqi, B., Poulos, M. G., James, D., et al. (2013). Molecular signatures of tissue-specific microvascular endothelial cell heterogeneity in organ maintenance and regeneration. *Dev. Cell* 26, 204–219. doi: 10.1016/j.devcel.2013.06.017

Olsavszky, V., Sticht, C., Schmid, C. D., Winkler, M., Wohlfeil, S. A., Olsavszky, A., et al. (2020). Exploring the transcriptomic network of multi-ligand scavenger receptor Stabilin-1- and Stabilin-2-deficient liver sinusoidal endothelial cells. *Gene* 768:145284. doi: 10.1016/j.gene.2020.145284

Pfaffl, M. W. (2001). A new mathematical model for relative quantification in real-time RT-PCR. *Nucleic Acids Res.* 29:e45. doi: 10.1093/nar/29.9.e45

Planas-Paz, L., Orsini, V., Boulter, L., Calabrese, D., Pikiolek, M., Nigsch, F., et al. (2016). The RSPO-LGR4/5-ZNRF3/RNF43 module controls liver zonation and size. *Nat. Cell Biol.* 18, 467–479. doi: 10.1038/ncb3337

Poisson, J., Lemoinne, S., Boulanger, C., Durand, F., Moreau, R., Valla, D., et al. (2017). Liver sinusoidal endothelial cells: Physiology and role in liver diseases. *J. Hepatol.* 66, 212–227. doi: 10.1016/j.jhep.2016.07.009

Preziosi, M., Okabe, H., Poddar, M., Singh, S., and Monga, S. P. (2018). Endothelial Wnts regulate beta-catenin signaling in murine liver zonation and regeneration: a sequel to the Wnt-Wnt situation. *Hepatol. Commun.* 2, 845–860. doi: 10.1002/hep4.1196

Profaci, C. P., Munji, R. N., Pulido, R. S., and Daneman, R. (2020). The blood-brain barrier in health and disease: important unanswered questions. *J. Exp. Med.* 217:e20190062. doi: 10.1084/jem.20190062

Rhee, S., Chung, J. I., King, D. A., D'amato, G., Paik, D. T., Duan, A., et al. (2018). Endothelial deletion of Ino80 disrupts coronary angiogenesis and causes congenital heart disease. *Nat. Commun.* 9:368. doi: 10.1038/s41467-017-02796-3

Rocha, A. S., Vidal, V., Mertz, M., Kendall, T. J., Charlet, A., Okamoto, H., et al. (2015). The angiocrine factor rspondin3 is a key determinant of liver zonation. *Cell Rep.* 13, 1757–1764. doi: 10.1016/j.celrep.2015.10.049

Sabbagh, M. F., Heng, J. S., Luo, C., Castanon, R. G., Nery, J. R., Rattner, A., et al. (2018). Transcriptional and epigenomic landscapes of CNS and non-CNS vascular endothelial cells. *Elife* 7:e36187. doi: 10.7554/eLife.36187.042

Sawane, M., Kajiya, K., Kidoya, H., Takagi, M., Muramatsu, F., and Takakura, N. (2013). Apelin inhibits diet-induced obesity by enhancing lymphatic and blood vessel integrity. *Diabetes* 62, 1970–1980. doi: 10.2337/db12-0604

Sawane, M., Kidoya, H., Muramatsu, F., Takakura, N., and Kajiya, K. (2011). Apelin attenuates UVB-induced edema and inflammation by promoting vessel function. *Am. J. Pathol.* 179, 2691–2697. doi: 10.1016/j.ajpath.2011.08.024

Schaffner, F., and Popper, H. (1963). Capillarization of hepatic sinusoids in man. *Gastroenterology* 44, 239–242. doi: 10.1016/S0016-5085(63)80130-4

Schledzewski, K., Geraud, C., Arnold, B., Wang, S., Grone, H. J., Kempf, T., et al. (2011). Deficiency of liver sinusoidal scavenger receptors stabilin-1 and−2 in mice causes glomerulofibrotic nephropathy via impaired hepatic clearance of noxious blood factors. *J. Clin. Invest.* 121, 703–714. doi: 10.1172/JCI44740

Shetty, S., Lalor, P. F., and Adams, D. H. (2018). Liver sinusoidal endothelial cells–gatekeepers of hepatic immunity. *Nat. Rev. Gastroenterol. Hepatol.* 15, 555–567. doi: 10.1038/s41575-018-0020-y

Srinivas, S., Watanabe, T., Lin, C. S., William, C. M., Tanabe, Y., Jessell, T. M., et al. (2001). Cre reporter strains produced by targeted insertion of EYFP and ECFP into the ROSA26 locus. *BMC Dev. Biol.* 1:4. doi: 10.1186/1471-213X-1-4

Stenman, J. M., Rajagopal, J., Carroll, T. J., Ishibashi, M., Mcmahon, J., and Mcmahon, A. P. (2008). Canonical Wnt signaling regulates organ-specific assembly and differentiation of CNS vasculature. *Science* 322, 1247–1250. doi: 10.1126/science.1164594

Subramanian, A., Tamayo, P., Mootha, V. K., Mukherjee, S., Ebert, B. L., Gillette, M. A., et al. (2005). Gene set enrichment analysis: a knowledge-based approach for interpreting genome-wide expression profiles. *Proc. Natl. Acad. Sci. U.S.A.* 102, 15545–15550. doi: 10.1073/pnas.0506580102

Tran, K. A., Zhang, X., Predescu, D., Huang, X., Machado, R. F., Gothert, J. R., et al. (2016). Endothelial beta-catenin signaling is required for maintaining adult blood-brain barrier integrity and central nervous system homeostasis. *Circulation* 133, 177–186. doi: 10.1161/CIRCULATIONAHA.115.015982

Walter, T. J., Cast, A. E., Huppert, K. A., and Huppert, S. S. (2014). Epithelial VEGF signaling is required in the mouse liver for proper sinusoid endothelial cell identity and hepatocyte zonation *in vivo*. *Am. J. Physiol. Gastrointest. Liver Physiol.* 306, G849–G862. doi: 10.1152/ajpgi.00426.2013

Wang, B., Zhao, L., Fish, M., Logan, C. Y., and Nusse, R. (2015). Self-renewing diploid Axin2(+) cells fuel homeostatic renewal of the liver. *Nature* 524, 180–185. doi: 10.1038/nature14863

Wang, Y., Sabbagh, M. F., Gu, X., Rattner, A., Williams, J., and Nathans, J. (2019). Beta-catenin signaling regulates barrier-specific gene expression in circumventricular organ and ocular vasculatures. *Elife* 8:e43257. doi: 10.7554/eLife.43257.035

Wild, S. L., Elghajiji, A., Grimaldos Rodriguez, C., Weston, S. D., Burke, Z. D., and Tosh, D. (2020). The canonical Wnt pathway as a key regulator in liver development, differentiation and homeostatic renewal. *Genes (Basel)* 11:1163. doi: 10.3390/genes11101163

Winkler, M., Staniczek, T., Kurschner, S. W., Schmid, C. D., Schonhaber, H., Cordero, J., et al. (2021). Endothelial GATA4 controls liver fibrosis and regeneration by preventing a pathogenic switch in angiocrine signaling. *J. Hepatol.* 74, 380–393. doi: 10.1016/j.jhep.2020.08.033

Wisse, E., De Zanger, R. B., Charels, K., Van Der Smissen, P., and Mccuskey, R. S. (1985). The liver sieve: considerations concerning the structure and function of endothelial fenestrae, the sinusoidal wall and the space of Disse. *Hepatology* 5, 683–692. doi: 10.1002/hep.1840050427

Wittlich, M., Dudek, M., Bottcher, J. P., Schanz, O., Hegenbarth, S., Bopp, T., et al. (2017). Liver sinusoidal endothelial cell cross-priming is supported by CD4 T cell-derived IL-2. *J. Hepatol.* 66, 978–986. doi: 10.1016/j.jhep.2016.12.015

Wohlfeil, S. A., Hafele, V., Dietsch, B., Schledzewski, K., Winkler, M., Zierow, J., et al. (2019). Hepatic endothelial notch activation protects against liver metastasis by regulating endothelial-tumor cell adhesion independent of angiocrine signaling. *Cancer Res.* 79, 598–610. doi: 10.1158/0008-5472.CAN-18-1752

Yokomori, H., Oda, M., Yoshimura, K., and Hibi, T. (2012). Enhanced expressions of apelin on proliferative hepatic arterial capillaries in human cirrhotic liver. *Hepatol. Res.* 42, 508–514. doi: 10.1111/j.1872-034X.2011.00945.x

Yu, G., Wang, L. G., Han, Y., and He, Q. Y. (2012). clusterProfiler: an R package for comparing biological themes among gene clusters. *OMICS* 16, 284–287. doi: 10.1089/omi.2011.0118

Zhang, L., Hoffman, J. A., and Ruoslahti, E. (2005). Molecular profiling of heart endothelial cells. *Circulation* 112, 1601–1611. doi: 10.1161/CIRCULATIONAHA.104.529537

Zhang, X. J., Olsavszky, V., Yin, Y., Wang, B., Engleitner, T., Ollinger, R., et al. (2020). Angiocrine hepatocyte growth factor signaling controls physiological organ and body size and dynamic hepatocyte proliferation to prevent liver damage during regeneration. *Am. J. Pathol.* 190, 358–371. doi: 10.1016/j.ajpath.2019.10.009

Zhou, Y., Wang, Y., Tischfield, M., Williams, J., Smallwood, P. M., Rattner, A., et al. (2014). Canonical WNT signaling components in vascular development and barrier formation. *J. Clin. Invest.* 124, 3825–3846. doi: 10.1172/JCI76431